

## Mechanics Properties on Glass Fiber Reinforced Polymer-Confined Concrete Short Columns†

JUAN WANG\*, JUNHAI ZHAO, QIAN ZHU and NAN LI

School of Civil Engineering, Chang'an University, Xi'an, Shaanxi Province, P.R. China

\*Corresponding author: Tel: +86 29 82337238; E-mail: wangjuanchd@126.com

AJC-15706

Based on the unified strength theory, considering the intermediate principal stress and the hooping effect of glass fiber reinforced polymer (GFRP) tube and stirrup to analyze the strength of concrete and section steel under triaxial compression, formulas of axial bearing capacities on two kinds of cross-section for GFRP-confined concrete short columns are proposed. By using nonlinear finite element ANSYS program, the establishment process of models is introduced in detail on such two types composite columns. Then, the axial ultimate bearing capacities and the complete stress-strain curves for members are obtained. In comparison with test results from the references, theoretical calculation results and numerical simulation results are satisfactory. Finally influences of loads on the stress distribution and the concrete strength and longitudinal reinforcement ratio on bearing capacities for members are studied.

**Keywords:** Unified strength theory, Nonlinear finite element, GFRP-confined concrete short columns, Axial ultimate bearing capacity.

### INTRODUCTION

Glass fiber reinforced polymer (GFRP)-confined concrete short column is a new kind of composite member composed of outer glass fiber reinforced polymer tube and inner reinforced concrete or inner steel-reinforced concrete, whose two common section forms are as shown in Fig. 1. The GFRP tube can not be subjected to pressure directly, but make concrete strength increased by the combined confinement effect with stirrups in horizontal. In order to avoid the longitudinal stress being transmitted to GFRP tube directly, there is always a proper gap left between the tube and the beam or at the column base, which also solves the connection details of casing concrete structure<sup>1</sup>. This composite member has so many merits to make itself widely used in the bridge construction and ocean engineering, such as good ductility of steel, lightweight, high strength and strong corrosion resistance of GFRP tube and high compressive strength of concrete, *etc.*<sup>2-5</sup>. Previous reports<sup>6,7</sup>, focus on the bearing capacities of GFRP tubed short columns filled with reinforced concrete (GFRP-RC) and GFRP tubed short columns filled with steel-reinforced concrete (GFRP-SRC) and have presented calculating formulas, but intermediate principal stress is not considered in the data regression method, simple superposition method and unified theory method they have adopted. In document<sup>8</sup>, it is not exact that steel rebar content

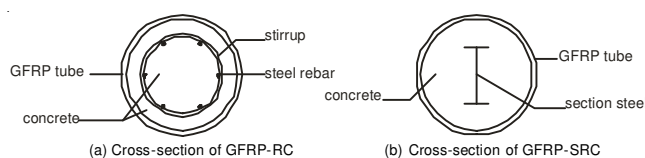


Fig. 1. Cross-section of GFRP-confined concrete short columns

is equivalent to the improvement of concrete strength. This article, based on the unified strength theory (UST), considering the intermediate principal stress to analyze their all components strength, deduces formulas of ultimate bearing capacities for such two types composite columns. Meanwhile, because of restrictions for test conditions, experimental research has some limitations on practice, sometimes people only obtain several discrete data with limited quantity which is difficult to use to directly show the result of the whole structure under the stress<sup>9</sup>. In order to gain further insight into the compressed properties and constraint mechanisms of such two types composite columns, the axial load behaviour of them are simulated by ANSYS software in this paper. Thereafter, the axial ultimate bearing capacities and the complete stress-strain relationship curves for members are gained. The analysis results are in good agreement with test results in document<sup>6</sup> and document<sup>7</sup>. This study provides theory basis for the application of such a composite structure.

†Presented at 2014 Global Conference on Polymer and Composite Materials (PCM2014) held on 27-29 May 2014, Ningbo, P.R. China

**Unified strength theory:** Based on the twin shear strength theory, a new strength theory was established by Yu in 1991 which considered the effects of intermediate principal stress  $\sigma_2$  and can be applied to a variety of different materials. Its mathematical expression can be expressed as<sup>10</sup>,

$$\sigma_1 - \frac{\alpha}{1+b} (b\sigma_2 + \sigma_3) = \sigma_t \quad \sigma_2 \leq \frac{\sigma_1 + \alpha\sigma_3}{1+\alpha} \quad (1a)$$

$$\frac{1}{1+b} (\sigma_1 + b\sigma_2) - \alpha\sigma_3 = \sigma_t \quad \sigma_2 \geq \frac{\sigma_1 + \alpha\sigma_3}{1+\alpha} \quad (1b)$$

In which,  $\sigma_1$ ,  $\sigma_2$ ,  $\sigma_3$  are maximum principal stress, intermediate principal stress and minimum principal stress of the unit, respectively;  $\alpha = \sigma_t/\sigma_c$  is the tension-compression strength ratio,  $\sigma_t, \sigma_c$  are the tensile yield strength and compressive yield strength of the material, respectively; Influence coefficient  $b$  ( $0 \leq b \leq 1$ ) shows intermediate principal stress has influence on material yield, which is called yield criterion coefficient.

**Calculation of axial compression bearing capacity:** Confinement effect of GFRP tube and stirrup on concrete: Constraint stress of stirrup on core-concrete is derived through force balance<sup>6</sup>,

$$\sigma_{sp} = \frac{2f_{yh}A_{sv1}}{sd_{co}} = \frac{\rho_{sv1}f_{yh}}{2} \quad (2)$$

In which,  $A_{sv1}$  is sectional area of single-limb stirrup;  $f_{yh}$  is yield strength of stirrup;  $s$  is stirrup spacing;  $d_{co}$  is diameter of concrete confined by stirrup;  $\rho_{sv1}$  is volume-stirrup ratio,

$$i.e., \rho_{sv1} = \frac{4A_{sv1}}{sd_{co}}$$

Constraint coefficient  $k_1$ <sup>11</sup> is adopted to take uneven restraint into account,

$$k_1 = \frac{\left(1 - \frac{s'}{2d_{co}}\right)^2}{1 - \frac{4A_s}{\pi d_{co}^2}} \quad (3)$$

In which  $s'$  is stirrup net spacing and  $A_s$  is sectional area of steel rebars.

Introducing reduction factor  $k_2$ <sup>6</sup> to transform restraint effect of stirrup on core-concrete to it on the total cross-section concrete,

$$k_2 = \frac{A_{co}}{A_c} = \left(\frac{d_{co}}{d_c}\right)^2 \quad (4)$$

In which,  $A_{co}$  is area of concrete confined by stirrup;  $A_c$  is area of total section concrete;  $d_c$  is the inside diameter of GFRP tube.

Combining (2), (3) and (4) we can get,

$$\sigma_{sp} = \frac{1}{2} k_1 k_2 \rho_{sv1} f_{yh} \quad (5)$$

Constraint stress of GFRP tube on concrete is solved,

$$\sigma_{gp} = \frac{2tf_{gt}}{d_c} \quad (6)$$

In which  $f_{gt}$ ,  $t$  are the loop tensile strength and thickness of GFRP tube, respectively.

**Axial compressive strength of concrete:** The concrete is under three-dimensional stress state, *i.e.*,  $0 > \sigma_1 = \sigma_2 > \sigma_3$ . Its axial compressive strength has increased due to the confinement effect of outer tube and stirrup. Based on the UST, stress of concrete is formulated as follows<sup>12</sup>,

$$\sigma_3 = f_c + k\sigma_1 \quad (7)$$

In which,  $k = (1 + \sin \varphi)/(1 - \sin \varphi)$ ,  $\varphi$  is concrete internal friction angle, the value of "k" varies from 1.0-7.0;  $\sigma_3$  is compressive strength of three-dimensional stress, *i.e.*  $f_c$ ;  $f_c$  is uniaxial compressive strength of concrete. We take  $f_c/f_{cu} = 0.84$  in this paper;  $\sigma_1$  is lateral pressure of the concrete. For GFRP-RC,  $\sigma_1 = \sigma_{sp} + \sigma_{gp}$  and for GFRP-SRC,  $\sigma_1 = \sigma_{gp}$ .

**Axial compressive strength of section steel:** The section steel of GFRP-SRC is under the stresses state of  $0 > \sigma_1 = \sigma_2 > \sigma_3$ , we can get,

$$\sigma_1 = \sigma_2 = \sigma_{gp} = \frac{2t}{d_c} f_{gt} \quad (8)$$

$$\sigma_3 = \frac{N_g}{A_g} \quad (9)$$

In which,  $A_g$ ,  $N_g$  are the sectional area and axial bearing capacity of section steel, respectively. For most of metal materials,

$\alpha = 1$ . Due to  $\frac{\sigma_1 + \alpha\sigma_3}{1+\alpha} < \frac{\sigma_1 + \sigma_2}{2} = \sigma_2$ , we substitute eqns. 8 and 9 into eqn. 1b, it can be expressed as,

$$\frac{1}{1+b} \left[ \left( \frac{2tf_{gt}}{d_c} \right) + b \left( \frac{2tf_{gt}}{d_c} \right) \right] - \frac{N_g}{A_g} = f_{gs} \quad (10)$$

In which  $f_{gs}$  is yield strength of section steel.

Accordingly, we can get axial bearing capacity of section steel,

$$N_g = \left( \frac{2tf_{gt}}{d_c} - f_{gs} \right) \times A_g \quad (11)$$

**Axial bearing capacity of GFRP-confined concrete short columns:** Assuming  $f_{y1}$  as yield strength of steel rebar, we can get axial bearing capacity of GFRP-RC,

$$N_1 = f'_c (A_c - A_s) + f_{y1} A_s$$

$$= \left[ f_c + k \left( \frac{1}{2} k_1 k_2 \rho_{sv1} f_{yh} + \frac{2tf_{gt}}{d_c} \right) \right] \times (A_c - A_s) + f_{y1} A_s \quad (12)$$

Combining eqns. 7 and 11, we can get the axial bearing capacity of GFRP-SRC,

$$N_2 = f'_c \times (A_c - A_g) + N_g = \left( f_c + \frac{2ktf_{gt}}{d_c} \right) \times (A_c - A_g) + \left( \frac{2tf_{gt}}{d_c} - f_{gs} \right) \times A_g \quad (13)$$

**Experimental verification:** The value of "k" in this paper is 3<sup>13</sup>. Substituting the correlative test data in document<sup>6</sup> and

document<sup>7</sup> into eqns. 12 and 13 to calculate, the comparisons between the calculation results and the test results of the documents are shown in Tables 1 and 2 below. In Table-1,  $f_{gt} = 430$  MPa,  $t = 5$  mm,  $d_c = 200$  mm.

**Constitutive model and failure criteria**

**Concrete:** The concrete is under the three-dimensional pressure state. Looking up the literatures home and abroad, Lam and Teng stress-strain model is adopted to define the concrete constitutive relation. This model is based on the strain database summarizing and analyzing the existing models and is proved to be simple and accurate by many scholars<sup>14</sup>.

Lam and Teng stress-strain model for GFRP-confined concrete expression is as follows:

$$\sigma = E_c \epsilon - \frac{(E_c - E_2)^2 \epsilon^2}{(4f'_{co})}, \quad 0 \leq \epsilon \leq \epsilon_t \tag{14a}$$

$$\sigma = f'_{co} + E_2 \epsilon, \quad \epsilon_t \leq \epsilon \leq \epsilon_{cc} \tag{14b}$$

In which,  $\epsilon_t = 2f'_{co}/(E_c - E_2)$ ,  $E_2 = 2f_1/\epsilon_{cc}$ ,  $f_1 = 2tf_{gt}/d_c$ ,  $\epsilon_{cc}/\epsilon_{co} = 1.75 + 22 \times (f_1/f'_{co})$ .  $E_c$ ,  $f'_{co}$  are elastic modulus and compressive strength of unconstrained concrete, respectively;  $E_2$  is the slope for the second section of the line segment;  $f_1$  is transverse restraining stress;  $\epsilon_{cc}$  is the axial strain corresponding to the peak stress of the confined concrete;  $E_g$  is loop elastic modulus of GFRP tube.

The failure criteria of the concrete used the Willam-Warnke five-parameter model. Steel rebar and section steel: Stress-strain curve of steel rebar can mainly be classified into five stages: elastic stage, elasto-plastic stage, plastic flow stage, hardening stage and secondary plastic flow stage. Mathematic expression is as follows,

$$\sigma = \begin{cases} E_s \epsilon & (\epsilon \leq \epsilon_e) \\ -A\epsilon^2 + B\epsilon + C & (\epsilon_e < \epsilon \leq \epsilon_{e1}) \\ f_{y1} & (\epsilon_{e1} < \epsilon \leq \epsilon_{e2}) \\ f_{y1} \left[ 1 + \frac{0.6 \times (\epsilon - \epsilon_{e2})}{(\epsilon_{e3} - \epsilon_{e2})} \right] & (\epsilon_{e2} < \epsilon \leq \epsilon_{e3}) \\ 1.6f_{y1} & (\epsilon > \epsilon_{e3}) \end{cases} \tag{15}$$

In which,  $A = 0.2f_{y1}/(\epsilon_{e1} - \epsilon_e)^2$ ,  $B = 2A\epsilon_{e1}$ ,  $C = 0.8f_{y1} + A(\epsilon_e)^2 - B\epsilon_e$ ,  $\epsilon_e = 0.8f_{y1}/E_s$ ,  $\epsilon_{e1} = 1.5\epsilon_e$ ,  $\epsilon_{e2} = 10\epsilon_e$ ,  $\epsilon_{e3} = 100\epsilon_e$ ;  $E_s$ ,  $f_u$  are elastic modulus and ultimate strength of steel, respectively. Von Mises yield criterion is taken as the yield function of steel rebar and section steel.

**GFRP tube:** This paper studies test specimens only considering the hoop tension of outer GFRP tube, results based on which are proved to be very closely to test results by article<sup>6</sup> and article<sup>8</sup>. As GFRP material can be approximated to be elastic, it has no yield strength. When the hoop tension reaches the ultimate tensile strength, GFRP tube is considered to break.

**Finite element model:** Unit type, real constant and material number attribute: Component parts of these two kinds of cross-section short columns are simulated by solid units according to actual size of related specimens in the literatures. SOLID65 unit is used to simulate concrete element, LINK8 unit is used to simulate steel rebar element, SOLID45 unit is used to simulate section steel element and SHELL41 membrane unit is used to simulate GFRP tube element. You can set the only tension option to fulfill the situation that GFRP tube element suffers only hoop tension without the axial compression. In addition, MASH200 unit is adopted to mesh surface grid.

TABLE-1  
MODEL SIZE OF GFRP-RC AND THE RESULTS COMPARISONS

No.	$f_{cu}$ (MPa)	$f_c$ (Mpa)	$d_{co}$ (mm)	$f_{yh}$ (N mm <sup>2</sup> )	$A_{sv1}$ (mm <sup>2</sup> )	$f_{y1}$ (N mm <sup>2</sup> )	$A_s$ (mm <sup>2</sup> )	$\rho_s$	$N_{exp}^a$ (kN)	$N_u^b$ (kN)	$N_{exp}/N_u$	$N_{ans}^c$ (kN)	$N_{exp}/N_{ans}$
A-1	37.5	31.5	0	0	0	0	0	0	3063.07	3015.93	1.0156	3064.02	0.9997
A-2	37.5	31.5	140	290	33.18	385	678.58	0.0216	3495.76	3217.26	1.0866	3358.04	1.0410
A-3	37.5	31.5	140	290	33.18	385	923.63	0.0294	3665.64	3288.13	1.1148	3426.90	1.0697
A-4	67.6	56.8	0	0	0	0	0	0	3632.98	3810.25	0.9535	3852.38	0.9430
A-5	67.6	56.8	140	290	33.18	385	678.58	0.0216	3720.27	3994.43	0.9314	3999.13	0.9303
A-6	67.6	56.8	140	290	33.18	385	923.63	0.0294	3852.78	4059.09	0.9492	4195.21	0.9184
A-7	64.1	53.8	0	0	0	0	0	0	3561.25	3717.89	0.9579	3726.82	0.9556
A-8	64.1	53.8	140	290	33.18	385	678.58	0.0216	3703.13	3904.06	0.9485	3989.73	0.9282
B-1	37.5	31.5	0	0	0	0	0	0	3117.08	3015.93	1.0335	3064.02	1.0173
B-2	37.5	31.5	140	290	33.18	385	678.58	0.0216	3533.44	3217.26	1.0983	3358.04	1.0522
B-3	67.6	56.8	0	0	0	0	0	0	3540.35	3810.25	0.9292	3852.38	0.9190
B-4	67.6	56.8	140	290	33.18	385	678.58	0.0216	3908.04	3994.43	0.9784	3999.13	0.9772

a.  $N_{exp}$  is test results in the document (6). b.  $N_u$  is results calculated by eqn. 12. c.  $N_{ans}$  is computed results by ANSYS.

TABLE-2  
MODEL SIZE OF GFRP-SRC AND THE RESULTS COMPARISONS

No.	$f_{gt}$ (MPa)	$f_{cu}$ (MPa)	$f_c$ (Mpa)	$t$ (mm)	$d_c$ (mm)	$f_{gs}$ (Mpa)	$A_g$ (mm <sup>2</sup> )	$A_c$ (mm <sup>2</sup> )	$N_{exp}^a$ (kN)	$N_u^b$ (kN)	$N_{exp}/N_u$	$N_{ans}^c$ (kN)	$N_{exp}/N_{ans}$
D-1	837.490	48.6	40.8	3	194	355	1430	29559.25	3220	2863.53	1.1245	3132.97	1.0278
D-2	837.597	48.6	40.8	3	194	355	1430	29559.25	3050	2863.81	1.0650	3132.98	0.9735
D-3	837.765	48.6	40.8	3	194	355	1430	29559.25	2600	2864.26	0.9077	2860.95	0.9088
D-4	488.674	48.6	40.8	5	190	355	1430	28352.87	2670	2705.57	0.9869	2850.27	0.9368
D-5	837.613	48.6	40.8	3	194	355	1430	29559.25	2875	2863.86	1.0039	3006.56	0.9562

a.  $N_{exp}$  is test results in the document<sup>7</sup>. b.  $N_u$  is results calculated by eqn. 13. c.  $N_{ans}$  is computed results by ANSYS.

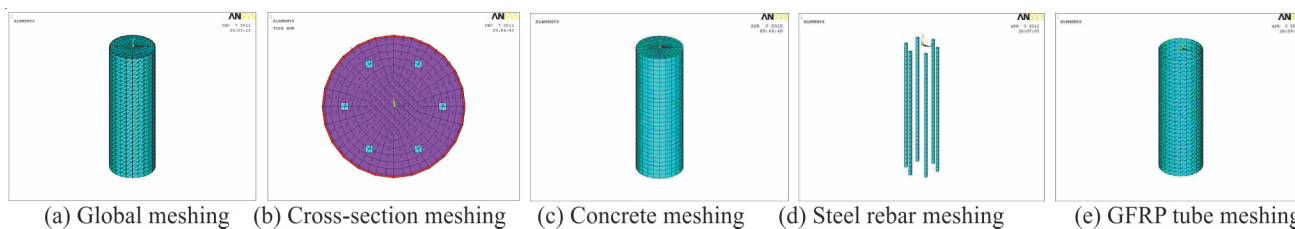


Fig. 2. Meshing results of finite element model for GFRP-RC

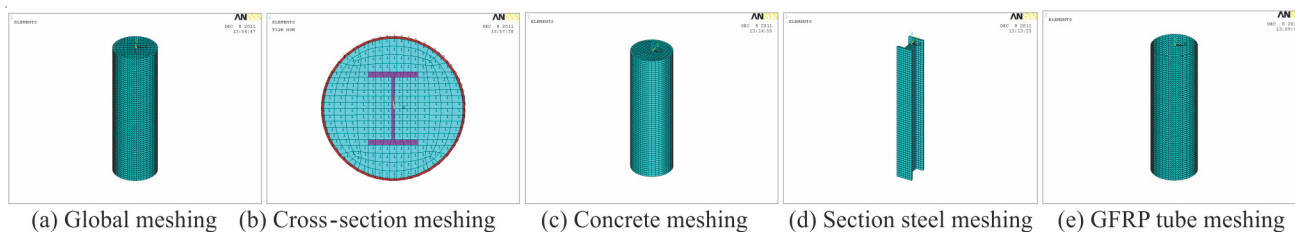


Fig. 3. Meshing results of finite element model for GFRP-SRC

Transforming stirrup content into volume-stirrup ratio of concrete, corresponding real constant of SOLID65 is established. For LINK8 unit, real constant representing area of steel rebar is set. Neither SOLID45 unit nor SHELL41 unit need to be set real constant.

The concrete, steel rebar and section steel are all isotropic materials. Elasticity modulus and Poisson's ratio of materials take the values according to material performance tests. The failure criteria of concrete uses Willam-Warnke five-parameter model in which the value of Shear Transferring Coefficient for close crack is 0.5 and the value of it for open crack is 0.9. While computing, we close the crush function to avoid difficulties from element freedom divergence caused by the crush of an individual element that will stop software computing. Multilinear isotropic hardening model is adopted in the simulation of concrete constitutive relation and multilinear kinematic hardening model is adopted in the simulation of constitutive relation for steel rebar, section steel and stirrup. As for GFRP tube, all we must do is to define the elastic modulus and Poisson's ratio.

**Establishment of models:** Discrete model was adopted for model establishment. As for GFRP-confined concrete short columns, there was no obvious difference in analysis results if friction is considered or not<sup>8,9</sup>. As the constraint effect of GFRP material on concrete is very strong, we assume GFRP tube, concrete and steel rebar or section steel are bonding fully with each other, the slip phenomena is not considered. GLUE option is set to bond the interfaces among these different types of elements.

After many contrasts of trial computations, appropriate unit sizes are chosen to make solution accurate and quick. To GFRP-RC, the total solid component is meshed into 7020 units, 5400 units are concrete, 180 units are steel rebar and 1440 units are GFRP tube. And then, To GFRP-SRC, the number of total units is 23520, 15600 units are concrete, 1440 units are section steel and 6480 units are the GFRP tube (Figs. 2 and 3).

In finite element models, we apply all DOF to nodes of the bottom for specimens and apply DOF in the X and Y directions to nodes on the top for them, with displacement

coupling in the Z direction. Displacement loading is exerted to the coupling node (Figs. 4 and 5).

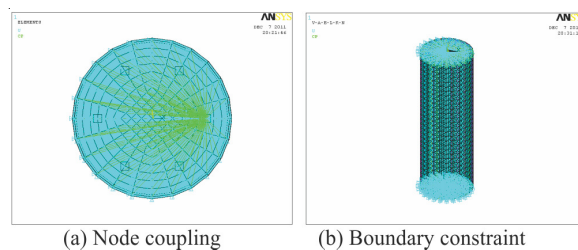


Fig. 4. Boundary conditions of GFRP-RC

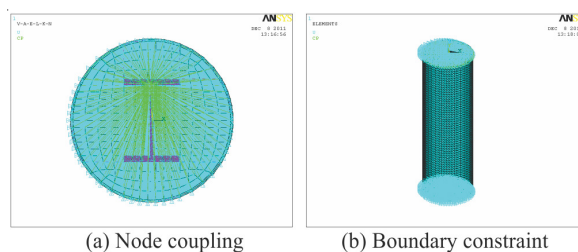


Fig. 5. Boundary conditions of GFRP-SRC

It is the loop tensile stress of the GFRP tube reaching the ultimate tensile strength that will mean the failure of the specimen and termination of the computation.

**Numerical analysis examples:** The comparisons between the axial ultimate bearing capacities of GFRP-RC and GFRP-SRC by finite element analysis and test results from document<sup>6</sup> and document<sup>7</sup> can be seen from Tables 1 and 2, respectively. The stress-strain curves of specimens obtained by simulation can be seen from Figs. 6 and 7.

Using specimen A-2 and specimen D-1 as examples, we can see deformation distribution and stress contour for various parts of models by simulation in Figs. 8 and 9.

Changing concrete strength  $f_{cu}$ , steel rebar ratio  $\rho_s$  and thickness of GFRP tube  $t$  to carry out numerical simulations for GFRP-RC, stress-strain curves and the influence of parameter,  $f_{cu}$ ,  $\rho_s$ ,  $t$  on the ultimate bearing capacity are shown in Figs. 10-12.

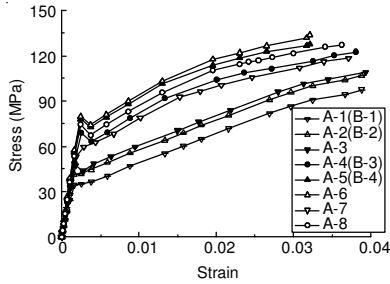


Fig. 6. Stress-strain curves of GFRP-RC

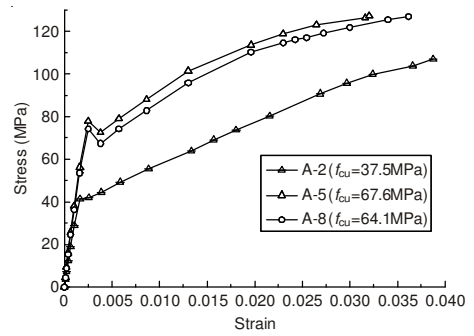


Fig. 10. Stress-strain curves of GFRP-RC with different steel rebar ratio

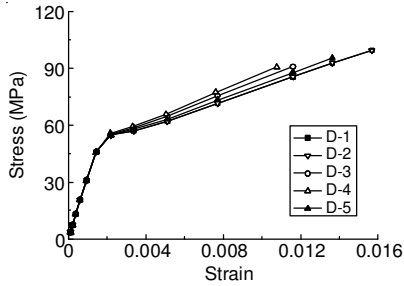


Fig. 7. Stress-strain curves of GFRP-SRC

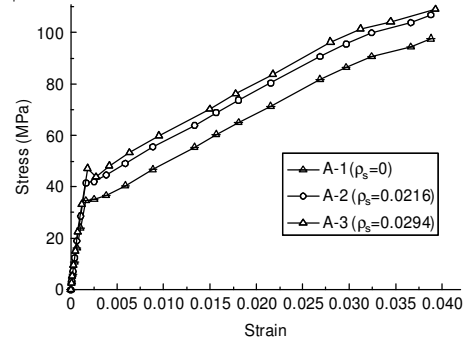


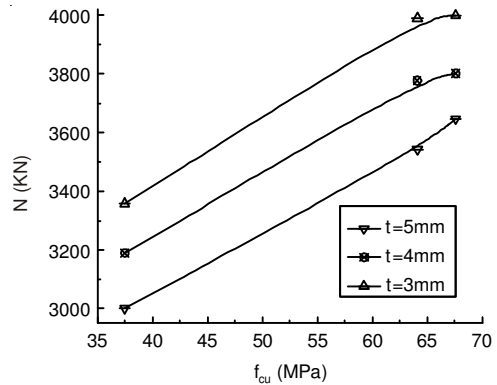
Fig. 11. Stress-strain curves of GFRP-RC with different concrete strength

**Conclusion**

This paper, based on the UST, considering the intermediate principal stress, has derived formulas of ultimate bearing capacities for GFRP-RC and GFRP-SRC and has simulated the stress-strain curves and stress fields of such two types composite columns using ANSYS.

It can be seen from Table-1 and 2 that the average ratios of test results to calculating values by eqns. 12 and 13 in this paper are 0.9997 and 1.0176, respectively. The ratios of test results to computed results by ANSYS for GFRP-RC are in the range of 0.9184-1.0697. Its average is 0.9793 and its mean square deviation is 0.0528. And the ratios of it for GFRP-SRC are in the range of 0.9088-1.0278. Its average is 0.9606 and its mean square deviation is 0.0399.

From Figs. 6 and 7, complete stress-strain curves for members can be seen intuitively. Besides, we can recognize



(a) Relations between  $f_{cu}$ ,  $t$  and  $N$

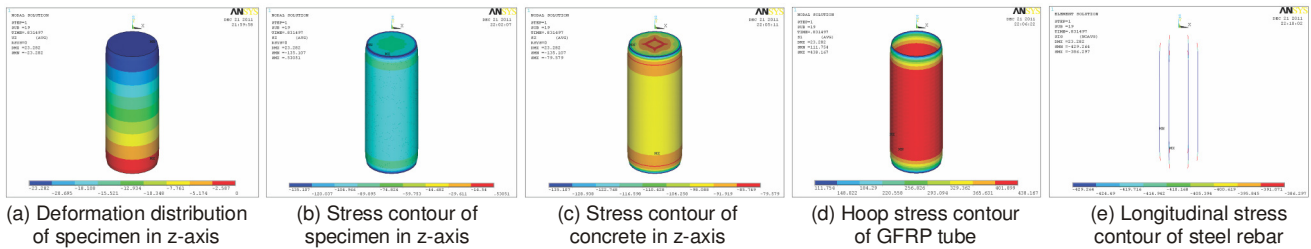


Fig. 8. Deformation distribution and stress contour of GFRP-RC

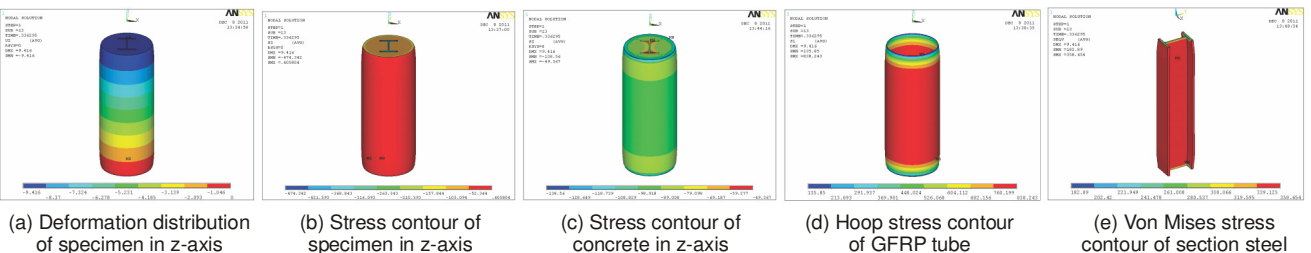


Fig. 9. Deformation distribution and stress contour of GFRP-SRC

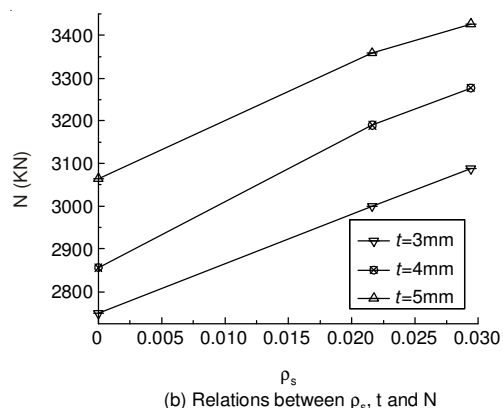


Fig. 12. Relations between related parameters and ultimate bearing capacities of GFRP-RC

that the axial compressive strengths of the concrete columns have been markedly improved due to the restriction of GFRP tube.

Through modifying the Zoom Factor, it can be seen from Figs. 8 and 9 when the specimens are destroyed, the middle deformation zone occurs obvious convex and the closer to the top of the member, the greater longitudinal displacement is. As shown in Fig. 8(d) and Fig. 9(d), the hoop tension suffered by the middle of GFRP tube is the largest clearly and decreases to the ends. As shown in Fig. 8(c) and Fig. 9(c) that the stress of concrete near GFRP tube is greater than it in the center section. In addition, we observe from Fig. 9(e) that while GFRP tube break, section steel are loaded evenly and have achieved the yield strength, the stress of which near the ends is the largest and collocates symmetrically. Under limit states, the stress of concrete all greatly exceeds the uniaxial compression strength. It shows that with the restriction of GFRP tube, concrete compression strength of either GFRP-RC or GFRP-SRC can be increased greatly. They are in line well with the experimental phenomenon of document<sup>6</sup> and document<sup>7</sup>.

The results lead to several conclusions:

(1) The theoretical values based on the UST and computed results of numerical simulation in this paper match well with test results and have reliable precision.

(2) Through numerical simulation, we can find that under limit states, the middle deformation of specimen is greater; the stress of concrete near GFRP tube is greater, but the distri-

bution of local stress of concrete has some differences due to different sectional forms of columns; when the hoop tension suffered by the middle of GFRP tube achieves ultimate tensile strength, the external concrete will crush first.

(3) Section steel are loaded evenly and have achieved the yield strength. Its maximum stress occurs at the section steel flange. With the restriction of GFRP tube, the concrete strength is increased greatly.

(4) As shown in Figs. 10-12, axial bearing capacities of GFRP-RC will be increased with concrete strength and steel rebar ratio.

Based on the analysis process and corresponding charts, the formulas of axial bearing capacities and the models proposed herein are proved correct and effective to get out the basic mechanic behaviours of these two different members through the whole loading progress.

#### ACKNOWLEDGEMENTS

This work reported herein is supported by the Fundamental Research Funds for the Central Universities (2014G5280010), the Natural Science Foundation of China (41202191) and Shaanxi Provincial Natural Science Foundation (2011JM7002).

#### REFERENCES

1. Y. Xiao, *China Civil Eng. J.*, **37**, 8 (2004).
2. J. Li, Y.D. Xue, *FRP/CM*, **7** (2004).
3. B.L. Chen and L.G. Wang, *Eng. Mechanics*, **30**, 178 (2013).
4. B.L. Chen and L.G. Wang, *Eng. Mechanics*, **29**, 355 (2012).
5. L. Zhou, C.Q. Wang, Q. Sun, H.C. Wang and X.L. Zhao, *J. Xi'an Jiaotong Univ.*, **47**, 112 (2013).
6. Q.X. Wang, B.F. Ruan and W.T. Cui, *J. Building Struct.*, **30**, 122 (2009).
7. B.L. Chen, G.P. Qin and L.G. Wang, *J. Northeastern Univ. (Nat. Sci.)*, **31**, 1035 (2010).
8. J. Wang, J.H. Zhao, Q. Zhu, S.S. Sun and Z. Liu, *Building Struct.*, **42**, 102 (2012).
9. N. Zhang, L.G. Wang and J.P. Wen, *J. Northeastern Univ. (Nat. Sci.)*, **34**, 1049 (2013).
10. M.H. Yu, *Unified Strength and Its Applications*, Springer-Verlag, Berlin (2004).
11. H. Li, *High-strength Concrete and Composite Structure*, Science Press, Beijing (2004).
12. J.H. Zhao, *Unified Strength Theory and Its Engineering Application*, Science Press, Beijing (2003).
13. F. Yu and D.T. Niu, *J. Harbin Institute Technol.*, **41**, 186 (2009).
14. J.G. Teng, J.F. Chen, S.T. Smith and L. Lam, *FRP Strengthened RC Structures*, China Building Industry Press, Beijing (2005).